LJMU Research Online

García-Bethencourt, G, Brook, CB, Grand, RJJ and Kawata, D

 A high fidelity Milky Way simulation with Kraken, Gaia-Enceladus, and Sequoia analogues: clues to their accretion histories

http://researchonline.ljmu.ac.uk/id/eprint/24444/

Article

For more information please contact researchonline@ljmu.ac.uk

A high fidelity Milky Way simulation with Kraken, Gaia-Enceladus, and Sequoia analogues: clues to their accretion histories

Guacimara García-Bethencourt [ID],[1,2]★ Chris B. Brook [ID],[1,2]★ Robert J. J. Grand [ID][1,2,3] and Daisuke Kawata [ID][4]

[1]*Universidad de La Laguna. Avda. Astrofísico Fco. Sánchez, La Laguna, Tenerife, Spain*
[2]*Instituto de Astrofísica de Canarias, Calle Via Láctea s/n, E-38206 La Laguna, Tenerife, Spain*
[3]*Astrophysics Research Institute, Liverpool John Moores University, 146 Brownlow Hill, Liverpool L3 5RF, UK*
[4]*Mullard Space Science Laboratory, University College London, Holmbury St. Mary, Dorking, Surrey RH5 6NT, UK*

ABSTRACT

Within a simulated Milky Way-like galaxy, we identify and analyse analogues of the Gaia-Enceladus (GE), Kraken, and Sequoia mergers that each matches remarkably well observational results, including in velocity and chemical abundance space, and their distributions in the j_z-Energy plane. The Kraken analogue is the earliest merger and has the highest total mass ratio. Consistent with previous studies, it is chemically indistinguishable from old *in situ* stars at the time of its accretion. The GE and Sequoia analogue events accrete at similar times in our simulation, both along filaments but from opposite sides of the main galaxy. The mean stellar ages of the GE and Sequoia analogues are both similar and, from our simulation results, we see that they can be separate entities and still naturally reproduce the observed properties of their stellar remnants at the present day, including the significant retrograde velocities of the Sequoia analogue remnant stars and the difference in the tracks of the two galaxies through chemical abundance space. Our results provide supporting information about the properties of these three merger events, and show for the first time that they can all be reproduced with a fully cosmological simulation, providing a possible self-consistent evolutionary pathway for the Milky Way's formation.

Key words: methods: numerical – galaxies: abundances – galaxies: evolution – galaxies: formation – galaxies: kinematics and dynamics.

1 INTRODUCTION

The formation and evolution of the Milky Way and its merger history is an active field of study, with detailed information provided in particular by the *Gaia* satellite (Gaia Collaboration et al. 2016, 2018). There is evidence that mergers have had an important impact on the development and growth of our Galaxy (e.g. Helmi et al. 2018). Merged satellite galaxies have left imprints of their accretion, especially in the stellar halo (e.g. Matsuno, Aoki & Suda 2019; Helmi 2020), meaning that details of mergers can be studied at the present day through their kinematics and/or chemical abundances, properties that are likely to remain nearly constant for long periods of time (e.g. Johnston, Hernquist & Bolte 1996; Johnston 1998; Helmi & White 1999). Analysis of chemical abundance ratios also provides information of the environment in which accreted stars were born, and hence, about the properties of their parent satellite galaxy (e.g. Freeman & Bland-Hawthorn 2002).

Several satellite accretion events have been identified in the Milky Way. For instance, the Sagittarius (Sgr) dwarf galaxy (Ibata, Gilmore & Irwin 1994), with a first passage into the Milky Way around 6 Grys ago (Ruiz-Lara et al. 2020), has left a stream of stars (Ibata et al. 2020; Vasiliev & Belokurov 2020) in an ongoing accretion process.

There is evidence of earlier merger events in the Milky Way. Gaia-Enceladus (GE; Helmi et al. 2018) or Gaia-Sausage (Belokurov et al. 2018) was accreted ∼10 Gyrs ago (see also Gallart et al. 2019; Chaplin et al. 2020) with an initial stellar mass of 5×10^8–5×10^9 $M_\odot$ (see also Mackereth et al. 2019; Vincenzo et al. 2019). This is believed to be the last significant merger of our Galaxy and was first identified as a stellar population with large radial motion, highly eccentric orbits, and low metallicity (Chiba & Beers 2000; Brook et al. 2003). GE dominates the region within the inner stellar halo, and a significant amount of its stellar debris is found in the solar neighbourhood, with a slight retrograde motion (Villalobos & Helmi 2008). GE stars have mean metallicities of [Fe/H] ~ -1.2 to -1.5 (e.g. Nissen & Schuster 2011) and low [α/Fe] values (e.g. Meza et al. 2005; Nissen & Schuster 2011; Haywood et al. 2018; Mackereth et al. 2019).

There is also evidence that the accretion of GE had a significant impact on the primitive Milky Way, when a fraction of stars in the primordial disc were heated (e.g. Zolotov et al. 2009; Gallart et al. 2019) to more halo-like kinematics. This event, known as the 'splash' (Belokurov et al. 2020), created an *in situ* population of 'hot thick disc' (Helmi et al. 2018; Di Matteo et al. 2019) stars.

★ E-mail: alu0100971361@ull.edu.es (GG-B); chbrook@ull.edu.es (CBB)

An even more ancient merger, dubbed Kraken (Massari, Koppelman & Helmi 2019; Kruijssen et al. 2020), has been proposed to explain the age–metallicity relation of globular clusters in the Milky Way. This early satellite has been estimated to have $M_\star \sim 2 \times 10^8$ $M_\odot$ at the time of infall, about 11 Gyrs ago (Kruijssen et al. 2020); less massive than GE. However, it might have been of great importance in the evolution of the Galaxy, due to a larger mass ratio between Kraken and the central galaxy at the time of its accretion. The remnant stars from Kraken are thought to have high binding energies, residing in the most inner parts of the Galaxy (Horta et al. 2021). The properties and even existence of Kraken are still quite uncertain, because its early accretion means that the stars have become mixed in phase space and cannot be easily identified using kinematics alone. Moreover, it has been suggested by Orkney et al. (2022) that the Kraken has similar chemical abundances than that of the main galaxy at the time of infall, and hence, it might also be difficult to identify through the analysis of chemical abundances. Conversely, a recent study by Horta et al. (2023a) advocates chemical distinction between Kraken/Heracles (Horta et al. 2021) and the low-metallicity *in situ* population of stars known as *Aurora* (Belokurov & Kravtsov 2022).

A smaller and later merger structure has been named Sequoia (Myeong et al. 2019), with an estimated stellar mass of $\sim 5 \times 10^7$ $M_\odot$ and accretion time around 9 Gyrs ago. Its stellar debris has mainly retrograde orbits and low binding energies, and is suggested to contribute to the retrograde motion found in the outer Galactic halo, along with GE (Helmi et al. 2017; Koppelman et al. 2019). Some debate has occurred regarding chemical abundances of Sequoia (Matsuno et al. 2019; Monty et al. 2020; Naidu et al. 2020) and whether it consisted of a single population, and whether it overlaps GE stars. A recent study (Matsuno et al. 2022) aimed to clear up this picture by using high-precision abundances, and found a clear separation between Sequoia and GE stars, with lower metallicity ([Fe/H]) and lower alpha element abundances, ([α/Fe]).

In this paper, we identify analogues of GE, Sequoia, and Kraken within a simulated Milky Way analogue galaxy. This Milky Way analogue has been shown to match a range of our Galaxy's observed properties, including detailed abundance patterns within the thick and thin discs, (Brook et al. 2020), the vertical and radial metallicity gradients (Miranda et al. 2016) of these populations, and the accreted and *in situ* halo population related to the 'splash' caused by the GE merger (Gallart et al. 2019). In this study, we explore the features of these three mergers in detail, including phase space velocities, energy-angular momentum, and chemical abundances, and find excellent agreement with the observed accreted satellites. This allows us to explore details of the mergers to provide hints on their sequence and information of their infall.

This paper is structured as follows: in Section 2 we present details of the simulation used for the study. In Section 3, we specify the main properties of each merger analogue, such as masses and accretion redshifts, kinematic phase space, chemical abundances, spatial distribution, star formation histories, and infall details. Next, Section 4 holds the discussion of these results, and in Section 5 we conclude and summarize the analysis and outcomes.

2 SIMULATION

2.1 The MaGICC simulations

The simulated galaxy of analysis is part of the MaGICC project (Brook et al. 2012; Stinson et al. 2012), a set of cosmological hydrodynamical simulations that reproduce observed galaxy scaling relations (Brook et al. 2012). These simulations are evolved with the smoothed particle hydrodynamics (Gingold & Monaghan 1977) code GASOLINE (Wadsley, Stadel & Quinn 2004).

Gas cooling is due to H, He, and several metal lines (Shen, Wadsley & Stinson 2010), including Compton and radiative cooling. Metal cooling uses CLOUDY (Ferland et al. 1998), and assumes an uniform UV ionizing radiation background (Haardt & Madau 1996). The diffusion of metals (e.g. C, O, Fe, Si, N, and Mg) is treated by using a turbulence mixing algorithm (Wadsley, Veeravalli & Couchman 2008).

Star formation processes take place in high-density regions, when gas reaches a temperature of $T < 10^4$ K and a density of $n_{th} < 9.3$ cm^{-3}. The Kennicutt–Schmidt law (Schmidt 1959; Kennicutt 1998) handles the amount of gas that is turned into stars:

$$\frac{\Delta M_\star}{\Delta t} = c_\star \frac{M_{gas}}{t_{dyn}}, \tag{1}$$

where $\Delta M_\star$ is the mass of each star particle formed, Δt is the timestep between star formation events, M_{gas} is the mass of the gas particles, $c_\star$ is the star formation efficiency, and t_{dyn} is the dynamical or free-fall time of the gas particles. The fraction of gas that is converted to stars during t_{dyn} is given by $c_\star = 0.167$. The SFR is $\rho_{gas}^{1.5}$, being ρ_{gas} the gas density.

The star particles formed are collisionless and represent clusters of co-eval stellar populations, with a Chabrier (Chabrier 2003) initial mass function.

Stellar feedback helps to regulate star formation in the system and is implemented via two different types. The first type refers to the early stellar feedback (Stinson et al. 2012), that accounts for the energetic radiation ejected by young massive stars before reaching the supernova phase. Also included is feedback due to type Ia supernovae (SNIa) and type II supernovae (SNII), that introduce energy and eject metals into the interstellar medium. The energy from supernovae is implemented via the blast-wave formalism (Stinson et al. 2006). Metals are ejected from both types of supernovae and via the stellar winds driven from asymptotic giant branch stars. This mass is distributed to the nearest neighbour gas particles through the smoothing kernel (Stinson et al. 2006).

Our Milky Way analogue is labelled g15784 from the MUGS set of galaxies (Stinson et al. 2010). At $z = 0$, there are ~ 4 million particles within the virial radius of $R_{vir} = 242$ kpc. The average mass of star, gas, and dark matter particles are: $M_{star, p} = 3.85 \times 10^4$ $M_\odot$, $M_{gas, p} = 2.05 \times 10^5$ $M_\odot$, and $M_{DM, p} = 1.11 \times 10^6$ $M_\odot$, respectively. The total, stellar and gas mass of the simulated galaxy (measured within R_{vir}) are the following: $M_{total} = 1.5 \times 10^{12}$ $M_\odot$, $M_\star = 8.28 \times 10^{10}$ $M_\odot$, and $M_{gas} = 13.50 \times 10^{10}$ $M_\odot$, respectively.

We use the AMIGA Halo Finder (AHF; Gill, Knebe & Gibson 2004; Knollmann & Knebe 2009) to identify and trace haloes. This process has uncertainties such as the frequency of the simulation outputs, which is ~ 0.214 Gyrs between snapshots, and it needs to be considered when interpreting the accretion redshifts of each merger.

The analysis is partly performed with the PYNBODY[1] package (Pontzen et al. 2013).

3 RESULTS

To obtain the stellar distributions and properties of each merger, we trace merged satellite galaxies since $z = 5.53$, the earliest snapshot,

[1] https://pynbody.github.io/pynbody/

following their evolution and disruption, when their stars become part of the central galaxy.

We identified three mergers that are analogues to proposed accreted structures in the Milky Way, namely: Kraken, GE, and Sequoia. The main properties of these analogue galaxies are shown in Table 1, and we will refer to them as sim_Kraken, sim_Enceladus, and sim_Sequoia. The total, stellar and gas masses are measured prior to the accretion, in the timestep at which the stellar mass of the mergers is maximum, $z_{\star max}$. The total mass ratio at $z_{\star max}$ between the merging satellite and the central galaxy is also shown in the table: sim_Kraken has the highest merger ratio, whilst sim_Enceladus is the most massive accreted satellite.

For further detail, $z_{\star merge}$ represents the redshift at which each merger can no longer be identified by the AHF, whilst at $z_{\star max}$ they are still separate haloes. Additionally, at $z_{\star merge}$ the stellar mass of the merger analogues has decreased due to stellar evolution and/or tidal stripping by the close interaction with the host galaxy.

In Table 1, we also include the approximate redshifts when the satellite analogues are spatially mixed within the host halo, i.e. their stars begin to form a spheroidal-like structure. Hence, this redshift, defined as z_{mixed}, is estimated visually from the stellar distribution of the mergers in coordinate space. It can be seen that this process requires a significant amount of time.

3.1 Kinematics and Integrals of Motion (IoM)

The velocity distributions at $z = 0$ in cylindrical coordinates are shown in Fig. 1. The left column represents the radial velocity in the plane (V_R) of the disc versus the rotational velocity (V_ϕ), the central column shows the velocity perpendicular to the disc (V_Z) versus V_ϕ, and the last column shows V_Z versus V_R. The sim_Kraken distribution has prograde rotation ($<v_\phi> = 74$ km s^{-1}), and large dispersion in all three velocity components. The sim_Enceladus shows the characteristically large radial velocities, and a small mean retrograde rotation of -5 km s^{-1}. For sim_Sequoia, we also see a large range of V_R, and more significant retrograde rotation ($<v_\phi> = -33$ km s^{-1}).

On the top panel of Fig. 2, we show the stellar distributions in the space defined by the total specific energy versus the specific z-component of the angular momentum, where each colour represents a different merger. The total energy is normalized to the maximum energy of all stars belonging to the main galaxy, so the limit of energetically bound stars is set to zero. We can see that sim_Kraken (in purple) has low energy and low angular momentum, with mean values of $(E_T, j_z) = (-2.6 \times 10^5$ km^2 s^{-2}, 1.7×10^2 kpc km s$^{-1})$. This is a result of the early accretion of the original satellite galaxy, as it was already close to the bottom of the potential well of the system at that time. There is scattering to higher energies, but all values are below -1.0×10^5 km^2 s^{-2}. The distribution of sim_Enceladus stars (in red) is found at $(E_T, j_z) = (-1.5 \times 10^5$ km^2 s^{-2}, 2.7×10^1 kpc km s$^{-1})$ in average. The region defined by this merger agrees with results from studies of observed GE stars (Koppelman et al. 2019; Massari et al. 2019; Ruiz-Lara et al. 2022). Lastly, sim_Sequoia has low binding energies and a relatively small dispersion. It also shows negative angular momentum, reflecting its retrograde rotational velocity. The mean values of energy and angular momentum of this merger are the following: $(E_T, j_z) = (-6.4 \times 10^4$ km^2 s^{-2}, -9.9×10^2 kpc km s$^{-1})$. These results are also consistent with the area populated by observed Sequoia stars in previous analysis (e.g. Massari et al. 2019; Wang et al. 2022).

Compared to Fig. 1, the identification of all three mergers is clearer in the space of the Integrals of Motion (IoM), since these are better conserved quantities.

The bottom panel of Fig. 2 shows the distributions of accreted stars at different redshift intervals. It clearly shows how accretions at different redshifts occupy different regions of the energy space. As well as the three accreted satellites focused on in this study, there is also a prograde structure of stars coloured in green. Although it is prominent in this plot, this merger is later and has lower mass than GE, with a stellar mass of 7.62×10^7 M$_\odot$ at $z_{\star max} = 1.76$.

We find that the sim_Enceladus event has an impact on previous accreted stellar structures in terms of their kinematics at the time of its infall (between $z = 2.87$ and $z = 2.65$). This effect is seen as an increase in the dispersion of the vertical velocity component (V_Z) of early accreted distributions. The implication is that the merger of sim_Enceladus 'splashed' *ex situ* stars, as well as splashing *in situ* forming (thick) disc stars into the halo (see also Grand et al. 2020).

3.2 Contribution of accreted stars to the galactic bulge and the solar region

We next study the contribution of accreted stars to the galactic bulge and to the solar neighbourhood at the present day. We define the inner bulge as a sphere with a radius of 2 kpc, while the outer bulge is defined as a concentric spherical layer between 2 and 3 kpc from the galactic centre. The solar region is defined as a spherical shell between 7 and 9 kpc. The results are displayed in Table 2, where each row contains the percentage of stars from each progenitor satellite that are found within the selected areas, along with the percentage that those stars represent with respect to the total stellar amount of each region.

More than half of the progenitor satellite of sim_Kraken is found in the inner 2 kpc of the simulated galaxy, whilst ∼14 per cent and ∼2 per cent of it is located in the outer bulge and solar region, respectively. However, the contribution of this merger to the present-day stellar populations is small at all radii, ranging in 0.01–0.05 per cent.

The later, more massive merger of sim_Enceladus is more extended in radial distance, and making larger contribution to the solar neighbourhood, having ∼11 per cent of its stars residing there. The contribution of sim_Enceladus to the innermost regions is relatively small. As for sim_Sequoia, it is even more radially extended, barely contributing to any of the selected areas, with only a ∼1 per cent of the original satellite within the solar region. These results reflect that later mergers with higher angular momentum contribute stars in more outer parts of the galaxy and are less bound (see also Fig. 2).

3.3 Stellar density profiles

In Fig. 3, we present the surface density profiles of the stars for the merger analogues at the present time. It is seen that sim_Kraken and sim_Enceladus have densities above 10^5 M$_\odot$ kpc^{-2} within 20 kpc from the centre of the galaxy, while the density of sim_Sequoia is under 10^4 M$_\odot$ kpc^{-2}. This is consistent with the results presented in Table 2, and shows that sim_Sequoia is more radially dispersed within the galaxy, and hence, it is more likely to contribute more to the outer regions, i.e. above 20 kpc. The stellar debris from sim_Kraken contributes to the oldest population of stars in the bulge (see Table 2), sim_Enceladus contributes to the bulge and inner halo, whilst sim_Sequoia tends to provide stars to the outer halo.

Table 1. Main properties of the sample of merger analogues. $z_{\star max}$ and $z_{\star merge}$ define the redshift before the accretion and the redshift where the merger begins, i.e. there is a close encounter with the central galaxy and significant disruption. Specifically, $z_{\star max}$ also defines the redshift at which the stellar mass of each merger is maximum. z_{mixed} is an approximate redshift at which the satellite stars have become disrupted and are spatially spread throughout the host galaxy's halo, and thus not in a spatially coherent configuration. The last row indicates the total mass ratio between the mergers and the main galaxy at $z_{\star max}$. All masses are calculated at $z_{\star max}$, except those marked with an asterisk (∗), which are measured at the time of peak total mass of sim_Sequoia ($z = 2.28$) so as to consider possible uncertainties due to tidal and ram pressure stripping during the merger's pericentric passage.

	Kraken	GE	Sequoia
$z_{\star max}$, $z_{\star merge}$	5.53, 4.79	2.87, 2.65	2.13, 1.88
z_{mixed}	∼ 2.87	∼ 1.57	∼ 0.82
M_{total} [$M_\odot$]	1.26×10^{10}	5.70×10^{10}	6.17×10^{9}∗
M_{stars} [$M_\odot$]	2.57×10^{7}	3.55×10^{8}	2.64×10^{7}
M_{gas} [$M_\odot$]	1.88×10^{9}	1.11×10^{10}	1.11×10^{9}∗
$M_{t, merger}/M_{t, main}$	0.306	0.145	0.009∗

3.4 Star formation histories

The top panel of Fig. 4 shows the average radial distance of the mergers from the galactic centre at each time. We indicate the positions of $z_{\star max}$ and $z_{\star merge}$ with vertical dashed lines and star-shaped marks, respectively. We also indicate the growth of the galaxy's viral radius in black. At the first output timestep recorded at redshift ∼5.5, sim_Kraken is already only 20 kpc from the central galaxy.

We also show the star formation histories of the three mergers in Fig. 4. The three lower panels display increasing star formation rates (SFRs) in a timespan of ∼3 Gyrs. The star formation history of these mergers suddenly stops after several peaks of high star formation activity, which could be caused by a compression of their gas during the process of accretion, as seen in Di Cintio et al. (2021). The cease in star formation coincides with the time of infall of sim_Kraken and sim_Enceladus, as indicated with the dashed lines in the panels. On the contrary, sim_Sequoia has its star formation halted less than 0.5 Gyrs before the accretion into the galaxy, that may indicate a loss of the gas reservoir by tidal or ram pressure stripping at that epoch (Simpson et al. 2018).

The average age of stars in the debris of the satellites is not only driven by infall time, but also by the SFR, with an increasing SFR causing the average age to be closer to the infall time whilst a steady SFR would mean the average age of stars is earlier. Thus, although sim_Sequoia has a later infall time than sim_Enceladus in this simulation, the average age of its stars are quite similar. Another effect that needs to be considered is that ongoing star formation may occur during the accretion of sim_Enceladus, which can also affect the calculation of accretion time from observed stellar ages (Di Cintio et al. 2021).

3.5 Chemical abundances: the [O/Fe] versus [Fe/H] plane

We explore the metallicities of the stars from our selection of merger analogues in the [O/Fe] versus [Fe/H] plane, as shown in Fig. 5. These chemical abundances are calculated prior to the accretion of each satellite galaxy, at $z_{\star max}$. Merged stars are shown as distributions of blue–green scale of contours, whilst the black–orange background represents the stars belonging to the main galaxy at each time. All contours are normalized so that they display the levels from 0.1 to 1.0 times their maximum density value.

We can see the distribution associated to sim_Kraken and the main galaxy in the first panel of the figure. These are placed
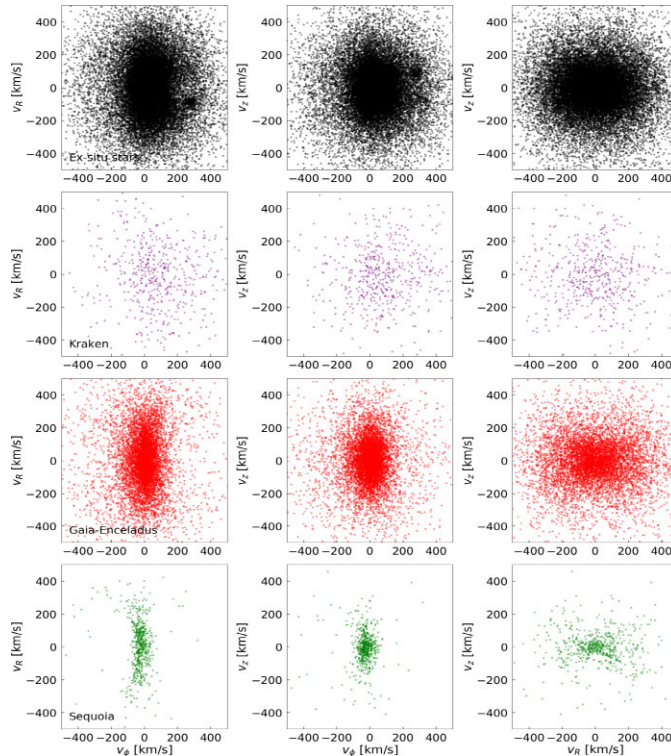

Figure 1. Distributions of stars in the three-dimensional velocity space at $z = 0$. From top to bottom, we show the distributions of all *ex situ* stars (in black), sim_Kraken (in purple), sim_Enceladus (in red), and sim_Sequoia (in green), respectively.
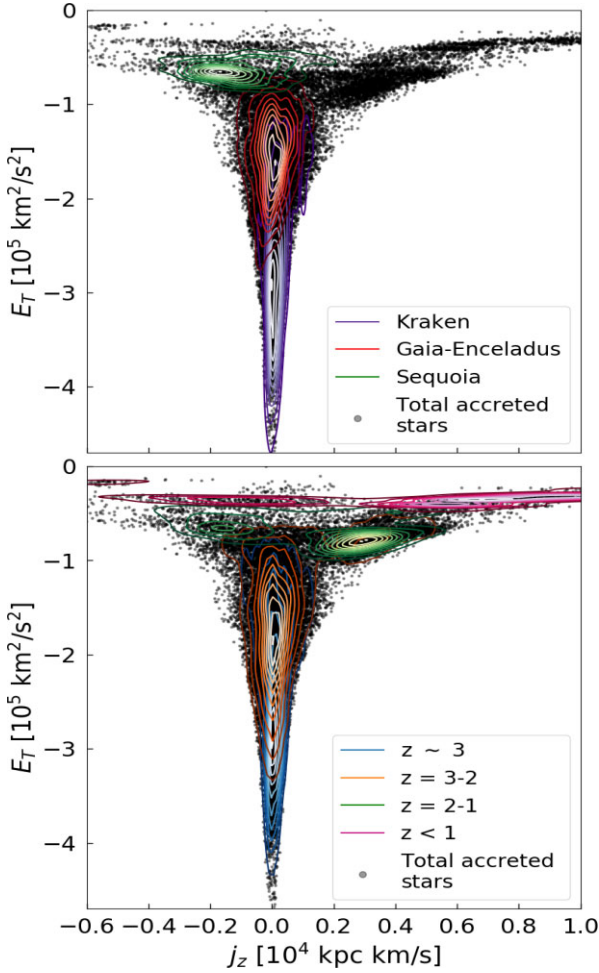
Figure 2. Distribution of accreted stars in IoM space at $z = 0$. We show the space defined by the total specific energy and z-component of the angular momentum. On the top panel, we present all *ex situ* stars (black), sim_Kraken (purple), sim_Enceladus (red), and sim_Sequoia (green). On the bottom panel, we show all *ex situ* stars (black), stars accreted at $z \sim 3$ (blue), stars accreted at $z = 3-2$ (orange), stars accreted at $z = 2-1$ (green), and stars accreted at $z < 1$ (pink). Contours are normalized to the maximum density value of each distribution and shown as fractions from 0.1 to 1.0.

Table 2. Percentage of stars from the various merged galaxies that end in the inner and outer bulge, and the solar region, and the percentage of stars in those regions that come from those merged galaxies.

	Inner bulge (0–2 kpc)	Outer bulge (2–3 kpc)	Solar region (7–9 kpc)
Kraken	54 per cent/0.02 per cent	14 per cent/0.05 per cent	2 per cent/0.01 per cent
GE	7 per cent/0.05 per cent	7 per cent/0.40 per cent	11 per cent/0.66 per cent
Sequoia	–	–	1 per cent/0.01 per cent

at low metallicities, with mean [Fe/H] of -2.77 and -2.49 dex, respectively. Both distributions show a high level of overlap, having little differences between them as discussed in Orkney et al. (2022) for the [Mg/Fe] versus [Fe/H] plane.

In the case of sim_Enceladus, the difference with the main progenitor in the [Fe/H] = [O/Fe] plain is clear, with just a small overlap, as is observed (e.g. Matsuno et al. 2022). As previously noted in Brook et al. (2020), the sim_Enceladus is accreted around half a Gyr earlier than the estimated time when the real GE was accreted into the Milky Way, meaning it is accreted with lower metallicity.
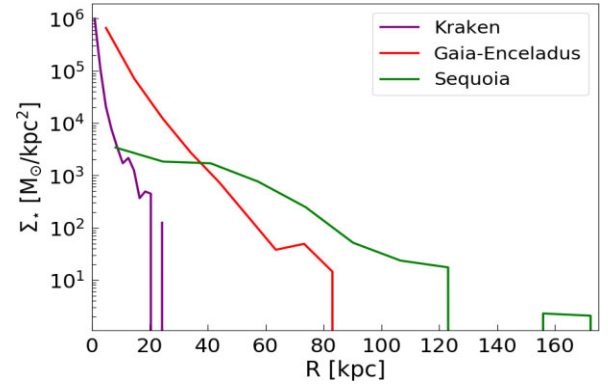

Figure 3. Surface density profiles of stars from the merger analogues with respect to the distance from the centre of the galaxy at $z = 0$.
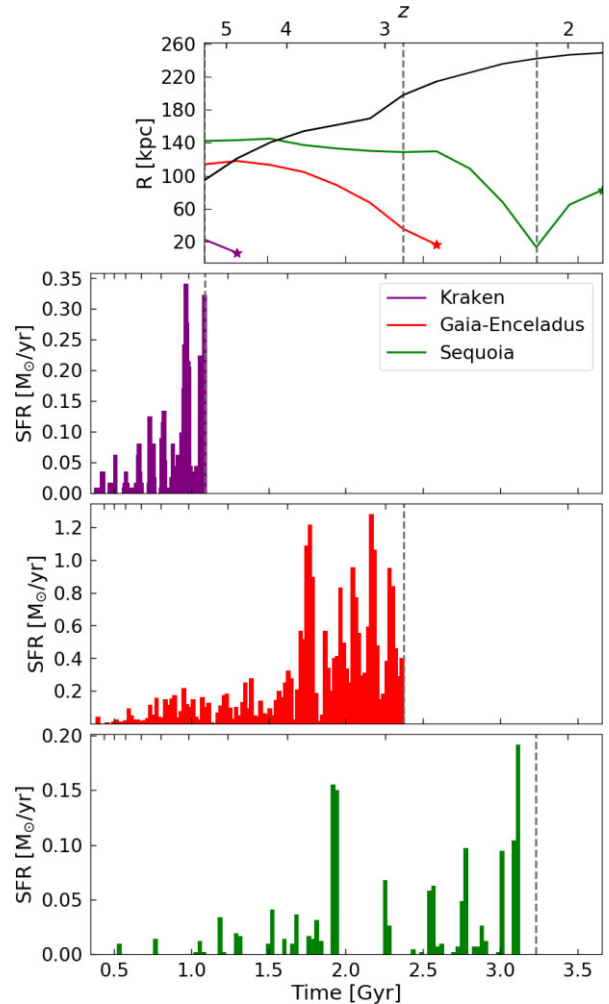

Figure 4. On the top panel, temporal evolution of the mean radial distance of stars belonging to sim_Kraken (purple), sim_Enceladus (red), and sim_Sequoia (green). The evolution of the virial radius of the galaxy is shown in black. The dashed vertical lines specify the redshift of maximum stellar mass prior to the accretion into the main system, this is at $z_{\star max}$. The star-shaped marks indicate the moment of the merger, i.e. $z_{\star merge}$. The lower panels show the star formation histories of the mergers measured at $z = 0$ and using a number of 100 bins.
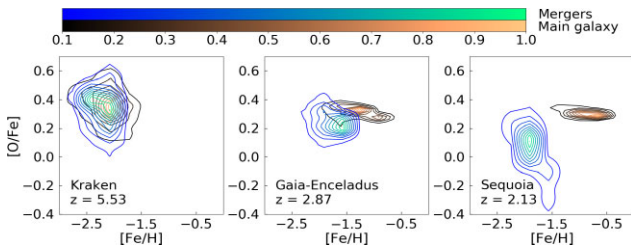
Figure 5. [O/Fe] versus [Fe/H] of stars from the main galaxy and from the mergers at their respective times of infall, $z_{\star max}$. From left to right, we show the sim_Kraken, sim_Enceladus, and sim_Sequoia distributions in blue–green contours. The black–orange background represents the stellar distribution of the main galaxy at each time. Contours are normalized to the maximum density value of each distribution individually, and shown from 0.1 to 1.0.

The offset from the main progenitor in [O/Fe]–[Fe/H] space is never the less clear in both the simulations and observations, which has been attributed to different star formation efficiencies of the main progenitor and the accreted galaxy (Brook et al. 2020).

For the last panel, we see that sim_Sequoia follows a different track in [Fe/H] = [O/Fe] space again, reflective of its lower mass and even lower star formation efficiency. The region covered by our sim_Sequoia distribution is in good agreement with the results presented in Matsuno et al. (2022) (see e.g. fig. 10). Here, they find a clear abundance distinction between Sequoia and GE of ∼0.1–0.2 dex, which is also consistent with our results.

As seen in Fig. 5, we also expect that these merger remnants follow different age–metallicity sequences as seen in Massari et al. (2019) and Kruijssen et al. (2020).

3.6 Accretion along filamentary structure

In Fig. 6, we show the two projections of the position of sim_Enceladus (red) and sim_Sequoia (green) stars at the time prior to the accretion of sim_Enceladus. On the top panel, the central galaxy is aligned face on, whilst in the bottom panel the central galaxy is aligned edge on. The background shows the gas density as shown on the colour bar on the right. The two satellites, sim_Enceladus and sim_Sequoia are both accreted from the most prominent filament of that epoch, but from opposite directions. This provides a possible explanation as to their similarly radial dominated orbits.

We note that, unlike sim_Enceladus and sim_Sequoia, which infall down the dominant filament in retrograde orbits, the prograde structure found in Fig. 2 is accreted along a less dense and less prominent filament.

4 DISCUSSION

In our simulation, sim_Kraken merges at a very early time, ending deep inside the potential well with its stars predominantly in the bulge according to the results presented in Table 2. As in other studies (e.g. Kruijssen et al. 2020; Orkney et al. 2022), our Kraken analogue is the most significant merger in terms of having the highest mass ratio. The early merger and short formation time prior is reflected in the high α abundances (Naidu et al. 2022). As also shown in Orkney et al. (2022), the failure to reach a downturn (or 'knee') in the [α/Fe]–[Fe/H] plane means that it is not possible to distinguish the abundances of Kraken from other stars forming in the central galaxy at the same time. None the less, it has to be considered that there may be certain differences from *in situ* stars in other non-alpha elements (e.g. Horta et al. 2021).
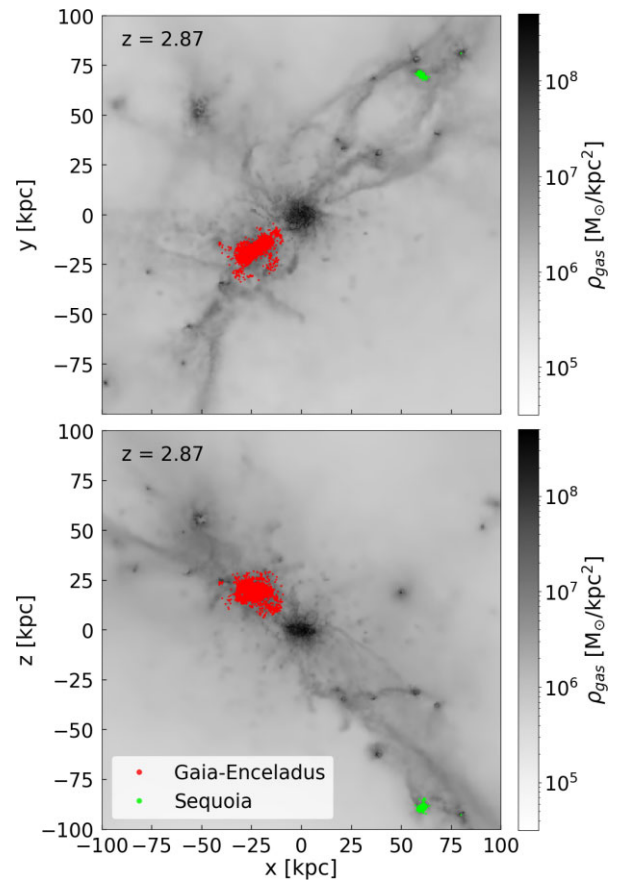

Figure 6. The position of sim_Enceladus (red) and sim_Sequoia (green) stars at the time prior to the accretion of sim_Enceladus. The background is the gas density, and shows that the two satellites are both accreted from the most prominent filament, but from opposite directions. The central galaxy is aligned face on (top panel) and edge on (bottom panel).

Particularly, this Kraken analogue is ∼10 times less massive in stars than that found in Kruijssen et al. (2020), and ∼100 times less massive than the Kraken-like merger studied in Orkney et al. (2022). Since the mass growth is large for early mergers, the accreted mass is strongly dependent on the redshift of accretion. However, it is important to consider that our sim_Kraken still matches the high α abundance distribution, together with the main progenitor, during this phase of rapid mass growth.

The accretion of sim_Enceladus in this simulation has been previously studied (Gallart et al. 2019; Brook et al. 2020). The accreted stars of sim_Enceladus resemble those of the observed GE in chemo-dynamical space, including the 'sausage' shape in the radial-rotational velocity plane (Belokurov et al. 2018) and downturn in the [α/Fe]–[Fe/H] plane.

Our simulated Milky Way accretes a sim_Sequoia analogue at a similar time as the sim_Enceladus, with the two satellites accreted from the same dominant filamentary structure but from opposite sides. This is an interesting result as it shows that the progenitor galaxies of GE and Sequoia are separate entities that seem to come from different origins in this simulation, which makes contrast with other studies that suggest that Sequoia was part of GE (e.g. Koppelman, Bos & Helmi 2020; Naidu et al. 2021; Amarante et al. 2022).

Additionally, in a recent work presented by An et al. (2022), a nearly in-plane collision between GE and the main galaxy is proposed

to explain the stellar distribution of this merger within the Milky Way. In our simulation, however, sim_Enceladus made its infall from above the galactic plane (as we can see on the bottom panel of Fig. 6), and yet, this analogue has proven to be well-matched to GE properties. What is perhaps the most interesting result in our study is the very close resemblance of these two simulated accreted satellites to the observed ones in the j_z-Energy plane (Fig. 2), including the significant retrograde motion of sim_Sequoia. Importantly, this series of accretion events occur within a fully CDM cosmological setting in which we simultaneously form a central galaxy with thin and thick discs, which also have been shown to closely match the observed Milky Way (Brook et al. 2020).

In addition, regions in the j_z-Energy plane defined by different groups of stars are shown to be consistent with respect to their merging time, i.e. there is a clear relation between the time of accretion and the final average energy of the stars. This relation has already been discussed in previous studies (e.g. Amorisco 2017; Pfeffer et al. 2020; Horta et al. 2023b).

In chemical abundance space, sim_Sequoia matches very well the observed Sequoia (Matsuno et al. 2022), with the downturn in [α/Fe]–[Fe/H] at a lower value of [Fe/H] than sim_Enceladus, reflecting its lower mass.

In our simulation, sim_Sequoia is accreted slightly after sim_Enceladus, although there is little difference in the average age of the stars of the two accreted satellites. We are not claiming that this reflects the real order of accretion of these satellites, but we do want to emphasize that the average ages of their stars depend on the details of their star formation history prior to their accretion, as well as on any ongoing star formation that may occur during accretion. Hence, phenomena such as the evolution of the gas density of mergers due to tidal stripping and ram pressure before and during the accretion, or the growth of the main galaxy with time, may play an important role in this process, and may depend on orbital parameters as well as mass.

5 CONCLUSIONS

We have presented the merger history of a fully cosmological Milky Way analogue simulation that has analogues of three key early merger events in the observed Milky Way, namely Kraken, GE, and Sequoia. The main results of this paper are summarized as follows:

(i) The three mergers characterized in this work are found to strongly match their observed properties, including their distributions in kinematic phase space and in IoM space. It is also observed a relation in which, early accreted stars tend to show lower energies and small rotation, whilst later structures have high energies and more prograde or retrograde motion.

(ii) We find very good agreement with the observed properties of the Sequoia merger, including its characteristic retrograde rotation in IoM space and its chemical abundances, being clearly separate from those of GE, which has higher values of [Fe/H] and [O/Fe] in average. This is a result that supports the high-precision abundances observed in Matsuno et al. (2022).

(iii) The results for our Kraken-like merger have close similarity with those from Orkney et al. (2022), in terms of being chemically indistinguishable from the main galaxy at the time of infall of this structure. Therefore, it overlaps populations of old *in situ* stars. This merger shows large dispersion in all three velocity components and resides in the innermost part of the galactic halo, being strongly bound to the system as well.

(iv) In this simulation, sim_Enceladus and sim_Sequoia have similar average ages: the latter is slightly younger because it is accreted later than the former. These analogues infall along the same dominant filament but from opposite directions. This provides a scenario where the two galaxies are distinct and did not infall together as part of a group.

We emphasize again that, presumably due to the similarities in merger history, this simulation has been shown to match a large range of chemo-dynamic properties of the real Milky Way including the chemo-dynamical properties of the thick and thin discs and stellar halo, as well as reproducing the remnants of a GE analogue. Simulated galaxies of similar mass using the same model but with different merger histories do not match nearly as well the properties of the Milky Way. Further, simulations using the same physical model has been shown to match a large range of scaling relations. The success of this model therefore provides support that, with the combined efforts of observations and simulations, we are arriving at a detailed understanding of the evolutionary history of our Galaxy within a cold dark matter cosmological framework.

Software: MATPLOTLIB (HUNTER 2007), NUMPY (HARRIS ET AL. 2020), PYNBODY (Pontzen et al. 2013), and SEABORN (Waskom 2021).

DATA AVAILABILITY

The data underlying this article is available upon request, chbrook@ull.edu.es.

REFERENCES

Amarante J. A. S., Debattista V. P., Beraldo e Silva L., Laporte C. F. P., Deg N., 2022, ApJ, 937, 12
Amorisco N. C., 2017, MNRAS, 464, 2882
An D., Beers T. C., Lee Y. S., Masseron T., 2022, ApJ, 952, 33
Belokurov V., Kravtsov A., 2022, MNRAS, 514, 689
Belokurov V., Erkal D., Evans N. W., Koposov S. E., Deason A. J., 2018, MNRAS, 478, 611
Belokurov V., Sanders J. L., Fattahi A., Smith M. C., Deason A. J., Evans N. W., Grand R. J. J., 2020, MNRAS, 494, 3880
Brook C. B., Kawata D., Gibson B. K., Flynn C., 2003, ApJ, 585, L125
Brook C. B., Stinson G., Gibson B. K., Wadsley J., Quinn T., 2012, MNRAS, 424, 1275
Brook C. B., Kawata D., Gibson B. K., Gallart C., Vicente A., 2020, MNRAS, 495, 2645
Chabrier G., 2003, PASP, 115, 763
Chaplin W. J. et al., 2020, Nature, 4, 382
Chiba M., Beers T. C., 2000, AJ, 119, 2843
Di Cintio A., Mostoghiu R., Knebe A., Navarro J. F., 2021, MNRAS, 506, 531
Di Matteo P., Haywood M., Lehnert M. D., Katz D., Khoperskov S., Snaith O. N., Gómez A., Robichon N., 2019, A&A, 632, A4

Ferland G. J., Korista K. T., Verner D. A., Ferguson J. W., Kingdon J. B., Verner E. M., 1998, PASP, 110, 761

Freeman K., Bland-Hawthorn J., 2002, ARA&A, 40, 487

Gaia Collaboration et al., 2016, A&A, 595, A1

Gaia Collaboration et al., 2018, A&A, 616, A1

Gallart C., Bernard E. J., Brook C. B., Ruiz-Lara T., Cassisi S., Hill V., Monelli M., 2019, Nature, 3, 932

Gill S. P. D., Knebe A., Gibson B. K., 2004, MNRAS, 351, 399

Gingold R. A., Monaghan J. J., 1977, MNRAS, 181, 375

Grand R. J. J. et al., 2020, MNRAS, 497, 1603

Haardt F., Madau P., 1996, ApJ, 461, 20

Harris C. R. et al., 2020, Nature, 585, 357

Haywood M., Di Matteo P., Lehnert M. D., Snaith O., Khoperskov S., Gómez A., 2018, ApJ, 863, 113

Helmi A., 2020, ARA&A, 58, 205

Helmi A., White S. D. M., 1999, MNRAS, 307, 495

Helmi A., Veljanoski J., Breddels M. A., Tian H., Sales L. V., 2017, A&A, 598, A58

Helmi A., Babusiaux C., Koppelman H. H., Massari D., Veljanoski J., Brown A. G. A., 2018, Nature, 563, 85

Horta D. et al., 2021, MNRAS, 500, 1385

Horta D. et al., 2023a, MNRAS, 520, 5671

Horta D. et al., 2023b, ApJ, 943, 158

Hunter J. D., 2007, Comput. Sci. Eng., 9, 90

Ibata R. A., Gilmore G., Irwin M. J., 1994, Nature, 370, 194

Ibata R., Bellazzini M., Thomas G., Malhan K., Martin N., Famaey B., Siebert A., 2020, ApJ, 891, L19

Johnston K. V., 1998, ApJ, 495, 297

Johnston K. V., Hernquist L., Bolte M., 1996, ApJ, 465, 278

Kennicutt R. C., Jr, 1998, ApJ, 498, 541

Knollmann S. R., Knebe A., 2009, ApJS, 182, 608

Koppelman H. H., Helmi A., Massari D., Price-Whelan A. M., Starkenburg T. K., 2019, A&A, 631, L9

Koppelman H. H., Bos R. O. Y., Helmi A., 2020, A&A, 642, L18

Kruijssen J. M. D. et al., 2020, MNRAS, 498, 2472

Mackereth J. T. et al., 2019, MNRAS, 482, 3426

Massari D., Koppelman H. H., Helmi A., 2019, A&A, 630, L4

Matsuno T., Aoki W., Suda T., 2019, ApJ, 874, L35

Matsuno T., Koppelman H. H., Helmi A., Aoki W., Ishigaki M. N., Suda T., Yuan Z., Hattori K., 2022, A&A, 661, A103

Meza A., Navarro J. F., Abadi M. G., Steinmetz M., 2005, MNRAS, 359, 93

Miranda M. S. et al., 2016, A&A, 587, A10

Monty S., Venn K. A., Lane J. M. M., Lokhorst D., Yong D., 2020, MNRAS, 497, 1236

Myeong G. C., Vasiliev E., Iorio G., Evans N. W., Belokurov V., 2019, MNRAS, 488, 1235

Naidu R. P., Conroy C., Bonaca A., Johnson B. D., Ting Y.-S., Caldwell N., Zaritsky D., Cargile P. A., 2020, ApJ, 901, 48

Naidu R. P. et al., 2021, ApJ, 923, 92

Naidu R. P. et al., 2022, preprint (arXiv:2204.09057)

Nissen P. E., Schuster W. J., 2011, A&A, 530, A15

Orkney M. D. A., Laporte C. F. P., Grand R. J. J., Gómez F. A., van de Voort F., Marinacci F., Pakmor R., Springel V., 2022, MNRAS, 517, L138

Pfeffer J. L., Trujillo-Gomez S., Kruijssen J. M. D., Crain R. A., Hughes M. E., Reina-Campos M., Bastian N., 2020, MNRAS, 499, 4863

Pontzen A., Roškar R., Stinson G., Woods R., 2013, Astrophysics Source Code Library, record ascl:1305.002

Ruiz-Lara T., Gallart C., Bernard E. J., Cassisi S., 2020, Nature, 4, 965

Ruiz-Lara T., Matsuno T., Sofie Lövdal S., Helmi A., Dodd E., Koppelman H. H., 2022, A&A, 665, 35

Schmidt M., 1959, ApJ, 129, 243

Shen S., Wadsley J., Stinson G., 2010, MNRAS, 407, 1581

Simpson C. M., Grand R. J. J., Gómez F. A., Marinacci F., Pakmor R., Springel V., Campbell D. J. R., Frenk C. S., 2018, MNRAS, 478, 548

Stinson G., Seth A., Katz N., Wadsley J., Governato F., Quinn T., 2006, MNRAS, 373, 1074

Stinson G. S., Bailin J., Couchman H., Wadsley J., Shen S., Nickerson S., Brook C., Quinn T., 2010, MNRAS, 408, 812

Stinson G. S., Brook C., Macciò A. V., Wadsley J., Quinn T. R., Couchman H. M. P., 2012, MNRAS, 428, 129

Vasiliev E., Belokurov V., 2020, MNRAS, 497, 4162

Villalobos Á., Helmi A., 2008, MNRAS, 391, 1806

Vincenzo F., Spitoni E., Calura F., Matteucci F., Silva Aguirre V., Miglio A., Cescutti G., 2019, MNRAS, 487, L47

Wadsley J. W., Stadel J., Quinn T., 2004, New A, 9, 137

Wadsley J. W., Veeravalli G., Couchman H. M. P., 2008, MNRAS, 387, 427

Wang F., Zhang H. W., Xue X. X., Huang Y., Liu G. C., Zhang L., Yang C. Q., 2022, MNRAS, 513, 1958

Waskom M. L., 2021, J. Open Source Softw., 6, 3021

Zolotov A., Willman B., Brooks A. M., Governato F., Brook C. B., Hogg D. W., Quinn T., Stinson G., 2009, ApJ, 702, 1058

This paper has been typeset from a TEX/LATEX file prepared by the author.